Received: 15 June 2021 | Revised: 21 September 2021 | Accepted: 20 October 2021

DOI: 10.1002/mma.7991

SPECIAL ISSUE PAPER

WILEY

Mathematical modeling of dendrite growth in an Al–Ge alloy with convective flow

Liubov V. Toropova[1,2] | **Markus Rettenmayr**[2] | **Peter K. Galenko**[2,3] | **Dmitri V. Alexandrov**[3]

[1]Laboratory of Mathematical Modeling of Physical and Chemical Processes in Multiphase Media, Department of Theoretical and Mathematical Physics, Ural Federal University, Ekaterinburg, Russian Federation

[2]Otto-Schott Institute for Materials Research, Friedrich Schiller University Jena, Jena, Germany

[3]Laboratory of Multi-Scale Mathematical Modeling, Department of Theoretical and Mathematical Physics, Ural Federal University, Ekaterinburg, Russian Federation

Correspondence
Liubov V. Toropova, Laboratory of Mathematical Modeling of Physical and Chemical Processes in Multiphase Media, Department of Theoretical and Mathematical Physics, Ural Federal University, Lenin ave., 51, Ekaterinburg 620000, Russian Federation.
Email: l.v.toropova@urfu.ru

Communicated by: I. Nizovtseva

Funding information
Ministry of Science and Higher Education of the Russian Federation, Grant/Award Number: 075-02-2021-1387; Russian Science Foundation, Grant/Award Number: 21-19-00279; Foundation for the Advancement of Theoretical Physics and Mathematics "BASIS", Grant/Award Number: 21-1-3-11-1

A theory of stable dendrite growth in an undercooled binary melt is developed for the case of intense convection. Conductive heat and mass transfer boundary conditions are replaced by convective conditions, where the flux of heat (or solute) is proportional to the temperature or concentration difference between the surface of the dendrite and far from it. The marginal mode of perturbation wavelengths is calculated using the linear morphological stability analysis. Combining this analysis with the solvability theory, we have derived a selection criterion that represents the first condition to define a combination of dendrite tip velocity and tip diameter. The second condition—the undercooling balance—is derived for intense convection. The theory under consideration determines the dendrite tip velocity and tip diameter for low undercooling. This convective theory is combined with the classical theory of dendritic growth (conductive boundary conditions), which is valid for moderate and high undercooling. Thus, the entire range of melt undercooling is covered. Our results are in good agreement with experiments on Al–Ge crystallization.

KEYWORDS

crystal anisotropy, dendrites, forced convection, mathematical modeling, phase transition, selection theory

MSC CLASSIFICATION

82B26

1 | INTRODUCTION

Dendrite growth in metastable (undercooled) liquids controls microstructure formation and composition of the solid phase for a variety of methods of directional and equiaxed solidification.[1–8] For example, depending on melt supercooling and solidification velocity, the formation of single crystals or a polycrystalline structure occurs.[9] The mechanisms of remelting of secondary dendrite arms strongly influence the structural features of the mushy zone during solidification

as well as the composition of the solid phase and the porosity.[10–17] Due to the impact of solidification on the properties of cast pieces, mathematical modeling of dendritic growth is a substantial area of contemporary science.

The problem of determining a stable mode of dendritic growth has been studied intensively over the past four decades. The paramount task of dendrite growth theory is to derive a microscopic solvability condition defining a stable solidification velocity V, which depends on the characteristic size ρ of the dendrite tip and the melt undercooling ΔT. One of the equations connecting V, ρ, and ΔT is the undercooling balance. In previous studies, it was solved for weakly anisotropic dendritic crystals growing slowly in pure liquids and binary alloy melts without convection as well as under conditions of forced convection in the direction of growth.[18–24] This theory was then extended to the cases of moderate and fast solidification velocities[25–27] and different crystal symmetries.[28,29] All these studies are devoted to mathematical modeling with boundary conditions implying conductive heat and mass transfer. It is well-known that in the case of (intense) natural convection, the fluxes of heat and solute at the solid/liquid interface differ from those predicted by the classical Fick law, i.e., the fluxes are not proportional to the gradients of heat and concentration of the dissolved solute; see among others[30–35]). In the presence of convection, we can use Newton's law of heat (mass) transfer, when the heat (solute) flux is proportional to the temperature (concentration) difference and the fluid flow velocity near the interface, i.e., the friction velocity).[30–35] In this paper, the conditions for a stable mode of growth of dendritic crystals under the condition of forced convection in an undercooled melt are derived. Such conditions occur, e.g., in undercooled droplets solidifying in electromagnetic levitation and in ice crystals growing in turbulent oceanic currents.[3,30–36] An important point is that the present theory, describing the case of intense convection in the melt, works at low undercooling where the classical conductive model differs from experiments (see, for example, experimental points for Al-24 at. % Ge mentioned below).

Let us especially clarify the terminology used in this paper concerning conductive and convective mechanisms of heat and mass transfer. The case of conductive mechanism is classical and well studied in previous works. It describes a motionless melt or forced laminar convection caused by a plane–parallel flow far from the growing crystal. On the other hand, the case of convective mechanism (intense convection) means either a turbulent flow or the flow before the transition to turbulence when the heat and mass fluxes become not Fickian. The mathematical model formulated and studied in this paper refers to the second case. The case of conductive-type boundary conditions was studied in many previous papers (see, among others, the review article by Alexandrov, Galenko, and Toropova[36]).

2 | MODEL

Let's analyze steady-state growth of two- and three-dimensional dendrites along the spatial axis z in the case of forced convective flow that comes from the direction opposite to the growth direction (Figure 1). First of all, we define the corresponding parabolic coordinates ξ, η (and φ in 3D geometry) connected to the Cartesian ones, x, y, and z, by the following expressions:

$$\begin{aligned} x = \rho\sqrt{\xi\eta},\ z = \frac{\rho(\eta-\xi)}{2} \quad &\text{two-dimensional (2D)},\\ x = \rho\sqrt{\xi\eta}\cos\varphi,\ y = \rho\sqrt{\xi\eta}\sin\varphi,\ z = \frac{\rho(\eta-\xi)}{2} \quad &\text{three-dimensional (3D)}, \end{aligned} \tag{1}$$

where ρ is the diameter of the dendrite tip, φ is the polar angle on the surface area perpendicular to the incoming flow, $\eta = 1$ defines the solid/liquid dendrite surface, 2D and 3D constitute the two- and three-dimensional space, respectively.

Basic model parameters are as follows: T_i represents the temperature at the solid/liquid interface, T_l and T_s are the temperatures in the liquid and solid phases, D_C and D_T are the solute diffusion coefficient and heat diffusivity, respectively, C_l is the solute concentration in the liquid, and $\mathbf{w}$ is the fluid velocity. The equations of convective heat and mass transfer in the liquid and conductive heat transfer in the solid are given as

$$\frac{\partial T_l}{\partial t} + (\mathbf{w}\cdot\nabla)\,T_l = D_T\nabla^2 T_l,\ \frac{\partial T_s}{\partial t} = D_T\nabla^2 T_s, \tag{2}$$

$$\frac{\partial C_l}{\partial t} + (\mathbf{w}\cdot\nabla)\,C_l = D_C\nabla^2 C_l. \tag{3}$$

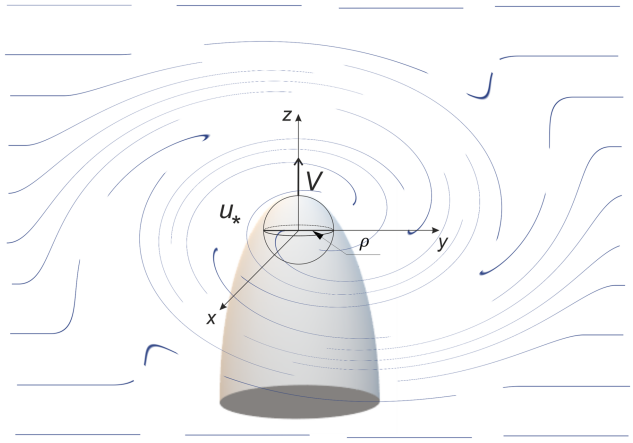

FIGURE 1 A sketch of local convection in front of dendrite tip. u_* represents friction velocity appearing as a result of intense heat and mass transfer

Heat and mass balance at the solid/liquid interface[30–33] read as

$$\frac{Q}{D_T c_p}\mathbf{v}\cdot\mathbf{n} = \nabla T_s\cdot\mathbf{n} + \frac{\alpha_h \rho_l c_l u_*}{k_s}\left(T_i - T_\infty\right), \tag{4}$$

$$\left(1-k_0\right)C_i\mathbf{v}\cdot\mathbf{n} = \alpha_m u_*\left(C_i - C_{l\infty}\right), \tag{5}$$

where Q is the latent heat, c_p is the heat capacity ($Q/c_p = T_Q$ is the hypercooling temperature, i.e., the temperature for complete adiabatic solidification), $\mathbf{v}\cdot\mathbf{n}$ is the normal growth velocity ($\mathbf{n}$ is the normal to the interface with unit length), α_h and α_m are the turbulence coefficients for heat and mass, respectively, ρ_l is the liquid phase density, c_l is specific heat capacity of the liquid phase, k_s is the solid phase thermal conductivity, and u_* is the friction velocity. The subscript i designates the temperature and solute concentration at the dendrite/liquid interface, and the subscript ∞ designates the temperature and solute concentration far away from dedrite tip.

The curvature of the solid/liquid interface at the vicinity of its tip is given by

$$\mathcal{K} = \begin{cases} 1/R, & \text{in 2D,} \\ (R_1+R_2)/(R_1R_2), & \text{in 3D,} \end{cases} \tag{6}$$

where R is the dendrite tip radius in 2D and R_1 and R_2 are the main curvature radii in 3D. The capillary length $d(\theta)$ and the function representing the anisotropic kinetics $\tilde{\beta}(\theta)$ are described by

$$d(\theta) = d_0\left\{1-\alpha_d\cos\left[n\left(\theta-\theta_d\right)\right]\right\}, \tag{7}$$

$$\tilde{\beta}(\theta) = \beta_0 T_Q\left\{1-\alpha_\beta\cos\left[n\left(\theta-\theta_\beta\right)\right]\right\}, \tag{8}$$

where d_0 and β_0 are the capillary and kinetic constants, respectively, $\alpha_d \ll 1$ is the interface stiffness depending on ϵ_c (i.e. a small surface energy anisotropy parameter), $\alpha_\beta \ll 1$ is the kinetic anisotropy parameter, θ_d and θ_β are the angles between the growth direction and the minimum functions $d(\theta)$ and $\tilde{\beta}(\theta)$, n is the order of the crystal symmetry. Note that Equations (7) and (8) were averaged over the polar angle.[36]

Consequently, the Gibbs–Thomson equation at the solid/liquid interface can be written as

$$T_i = T_l = T_s = T_0 - mC_l - T_Q d(\theta)\mathcal{K} - \tilde{\beta}(\theta)\mathbf{v}\cdot\mathbf{n}, \tag{9}$$

where T_0 is the melting temperature of a single-component melt at a planar interface, and m represents the slope of the liquidus line.

Rewriting the heat transfer equation (2) and the boundary conditions (4) in parabolic and paraboloidal coordinates (1) and integrating them, we find the temperature distributions in 2D and 3D growth geometries by analogy with the classical case of conductive-type boundary conditions[36]

$$T_l(\eta) = T_i + (T_\infty - T_i)\frac{I_T(\eta)}{I_T(\infty)}, \tag{10}$$

where $I_T(\eta)$ can be written as

$$I_T(\eta) = \begin{cases} \int_1^\eta \frac{\exp(-P_g\eta')}{\sqrt{\eta'}}d\eta', & \text{in 2D case,} \\ \int_1^\eta \frac{\exp(-P_g\eta')}{\eta'}d\eta', & \text{in 3D case.} \end{cases} \tag{11}$$

For the same transformation steps with the diffusion equation, we obtain

$$C_l(\eta) = C_i + (C_{l\infty} - C_i)\frac{I_C(\eta)}{I_C(\infty)}, \tag{12}$$

where $I_C(\eta)$ reads as

$$I_C(\eta) = \begin{cases} \int_1^\eta \frac{\exp(-P_C\eta')}{\sqrt{\eta'}}d\eta', & \text{in 2D case,} \\ \int_1^\eta \frac{\exp(-P_C\eta')}{\eta'}d\eta', & \text{in 3D case.} \end{cases} \tag{13}$$

Here, $P_g = \rho V/(2D_T)$ and $P_C = \rho V/(2D_C)$ denote the Péclet numbers for the temperature and concentration fields, respectively (V is the steady-state dendrite growth velocity).

To find the interfacial temperature T_i and solute concentration C_i, we rewrite conditions (4) and (5) for the isothermal crystal $T_s = \text{const.}$ in the form of

$$\frac{T_Q V}{D_T} = \frac{\alpha_h \rho_l c_l u_*}{k_s}, (1-k_0)C_i V = \alpha_m u_*(C_i - C_{l\infty}).$$

Now expressing T_i and C_i, we get

$$T_i = T_\infty + \frac{T_Q V k_s}{\alpha_h \rho_l c_l u_* D_T}, \tag{14}$$

$$C_i = \frac{\alpha_m u_* C_{l\infty}}{\alpha_m u_* - (1-k_0)V}. \tag{15}$$

3 | LINEAR STABILITY ANALYSIS

Let us now select the marginal mode of morphological perturbations wavenumber imposed on the dendrite surface, which is required for the solvability theory developed in Section 4. For this purpose, we assume that the solid/liquid interface is perturbed as is schematically shown in Figure 2. Note that analytical solutions describing steady-state dendritic growth can be found from the stationary solutions (10)–(15) in the case of small anisotropies of surface energy and growth kinetics. In order to find the limiting (marginal) wavenumber k_m in analogy with the conductive theory,[36] a linear stability analysis is developed below for convective heat and mass transfer.

We introduce a special coordinate system (x_c, y_c) which is related to the dendrite surface, and x_c and y_c denote the tangent and normal axes to the dendrite surface.[22,36] Also note that the origin of this coordinate system is on the dendrite surface, and θ represents the angle between the surface normal and the growth axis. Thus, small perturbations of the temperature and solute concentration fields that follow from (2) and (3) satisfy the equations

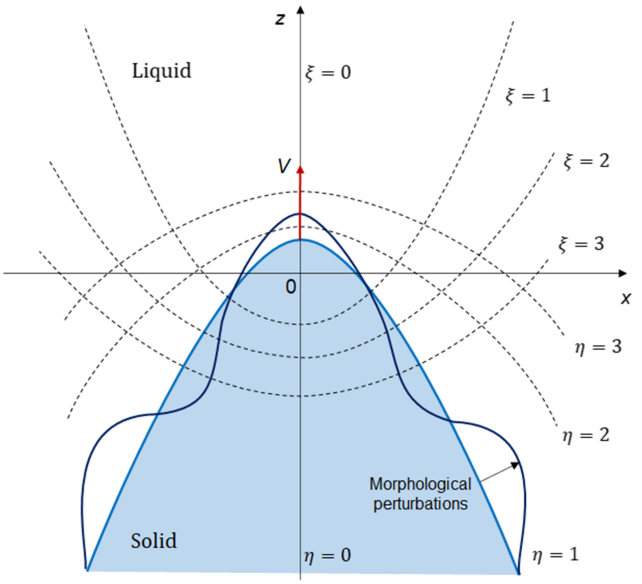

FIGURE 2 A 2D sketch of morphological perturbations on the dendrite surface

$$\begin{aligned}\frac{\partial T'_{l,s}}{\partial t}+\bar{u}\frac{\partial T'_{l,s}}{\partial x_c}+\bar{v}\frac{\partial T'_{l,s}}{\partial y_c}+v'\frac{d\bar{T}_{l,s}}{dy_c}&=D_T\nabla^2 T'_{l,s},\\ \frac{\partial C'_l}{\partial t}+\bar{u}\frac{\partial C'_l}{\partial x_c}+\bar{v}\frac{\partial C'_l}{\partial y_c}+v'\frac{d\bar{C}_l}{dy_c}&=D_C\nabla^2 C'_l.\end{aligned} \tag{16}$$

Since the fluid velocity far from the crystal is zero (intense liquid flow is characterized only by the friction velocity u_* near the dendrite), the steady-state unperturbed fluid velocity components[36] $\bar{u}$ and $\bar{v}$ only have the main contributions, i.e. $\bar{u}=-V\sin\theta$ and $\bar{v}=-V\cos\theta$.

Perturbations of the temperature fields T'_l and T'_s in the liquid and solid phases, solute concentration C'_l and dendrite surface ξ' can be represented in the form of oscillating functions because any real perturbation can be expanded in a series of such functions. So, accordingly to the classical perturbation theory,[22,36] we have

$$\begin{aligned}T'_l(x_c,y_c,t)&=(T_{l0}+T_{l1}y_c+T_{l2}y_c^2)\exp(\omega t+ikx_c-\epsilon k y_c),\\ T'_s(x_c,y_c,t)&=(T_{s0}+T_{s1}y_c+T_{s2}y_c^2)\exp(\omega t+ikx_c-\epsilon k y_c),\\ C'_l(x_c,y_c,t)&=(C_{l0}+C_{l1}y_c+C_{l2}y_c^2)\exp(\omega t+ikx_c-\epsilon k y_c),\\ \xi'(x_c,y_c,t)&=C\exp(\omega t+ikx_c-\epsilon k y_c),\end{aligned} \tag{17}$$

where $\partial\xi'/\partial t=-v'$, $T_{l\iota}$, $T_{s\iota}$, C_ι, and C stand for the perturbation amplitudes ($\iota=0,1,2$), and ω and k are the frequency and wavenumber of the perturbations, respectively, i is an imaginary unit, and $\epsilon=1$ or -1 (its sign is given by the sign of the real part of k, as disturbances cannot be diverging). Let us especially emphasize that the perturbation amplitudes (17) are polynomials of the second order, as was proved in the previously developed theory.[9] Also, note that disturbances can be caused by any physical process or phenomenon that accompanies dendritic growth (e.g., mechanical disturbance, temperature or fluid velocity fluctuations).

Combining Equations (16) and (17), we arrive at the following amplitudes

$$\begin{aligned}T_{l,s1}&=\frac{3\omega C}{4\epsilon k D_T}\frac{d\bar{T}_{l,s}}{dy_c}-\frac{\left[\omega+Vk(\epsilon\cos\theta-i\sin\theta)\right]T_{l,s0}}{2\epsilon k D_T},\quad T_{l,s2}=\frac{\omega C}{4D_T}\frac{d\bar{T}_{l,s}}{dy_c},\\ C_1&=\frac{3\omega C}{4\epsilon k D_C}\frac{d\bar{C}_l}{dy_c}-\frac{\left[\omega+Vk(\epsilon\cos\theta-i\sin\theta)\right]C_0}{2\epsilon k D_C},\quad C_2=\frac{\omega C}{4D_C}\frac{d\bar{C}_l}{dy_c},\end{aligned} \tag{18}$$

where

$$\left.\frac{d\bar{T}_l}{dy_c}\right|_{y_c=0} = -\frac{2T_Q V k_s \exp(-P_g)}{\rho\alpha_h \rho_l c_l u_* D_T I_T(\infty)} \equiv h_1,$$
$$\left.\frac{d\bar{C}_l}{dy_c}\right|_{y_c=0} = -\frac{2(1-k_0)VC_{l\infty}\exp(-P_C)}{\rho\left[\alpha_m u_* - (1-k_0)V\right] I_C(\infty)} \equiv h_2. \tag{19}$$

Expanding expressions (4), (5), and (9) into series at the dendrite surface $y_c = 0$, we arrive at four equations for morphological perturbations

$$T_l' = -(h_1 + mh_2)\xi' - mC_l' - dT_Q\frac{\partial^2\xi'}{\partial y_c^2} + \tilde{\beta}\frac{\partial\xi'}{\partial t},$$
$$T_s' = mh_2\xi' + mC_l' + dT_Q\frac{\partial^2\xi'}{\partial y_c^2} - \tilde{\beta}\frac{\partial\xi'}{\partial t},$$
$$\frac{T_Q}{D_T}\frac{\partial\xi'}{\partial t} = \frac{\partial T_s'}{\partial y_c} - \frac{\alpha_h\rho_l c_l u_*}{k_s}h_1\xi' - \frac{\alpha_h\rho_l c_l u_*}{k_s}T_l', \tag{20}$$
$$\frac{1-k_0}{\alpha_m u_*}\left(V\cos\theta C_l' + V\cos\theta h_2\xi' + C_i\frac{\partial\xi'}{\partial t}\right) + C_l' + h_2\xi' = 0.$$

Let us explain in detail how to derive these expressions using the first equation as an example. Equation (9) gives at $y_c = 0$

$$T_l = T_0 - mC_l - T_Q d(\theta)\mathcal{K} - \tilde{\beta}(\theta)\mathbf{v}\cdot\mathbf{n}. \tag{21}$$

The steady-state (unperturbed) two-dimensional case leads to

$$\bar{T}_l = T_0 - m\bar{C}_l - \frac{dT_Q}{R} - \tilde{\beta}V. \tag{22}$$

Now expanding the temperature and concentration in series

$$T_l = \bar{T}_l + T_l' + \left.\frac{d\bar{T}_l}{dy_c}\right|_{y_c=0}\xi',\ C_l = \bar{C}_l + C_l' + \left.\frac{d\bar{C}_l}{dy_c}\right|_{y_c=0}\xi'$$

and taking

$$\mathbf{v}\cdot\mathbf{n} = V + v',\ v' = -\frac{\partial\xi'}{\partial t}$$

into account, we obtain from (21)

$$\bar{T}_l + T_l' + \left.\frac{d\bar{T}_l}{dy_c}\right|_{y_c=0}\xi' = T_0 - m\bar{C}_l - mC_l' - m\left.\frac{d\bar{C}_l}{dy_c}\right|_{y_c=0}\xi' - dT_Q\left(\frac{1}{R} + \left.\frac{\partial^2\xi'}{\partial y_c^2}\right|_{y_c=0}\right) - \tilde{\beta}\left(V + v'\right).$$

Note that only linear terms in perturbations have been taken into account. Now keeping in mind the steady-state boundary condition (22) and designations (19), we come to the first line of equations (20). The remaining lines of (20) can be obtained by similar transformations.

Substituting perturbations (17) into the boundary conditions (20), we get four equations for the perturbation amplitudes T_{l0}, T_{s0}, C_0 and C

$$
\begin{aligned}
T_{l0} &= -(h_1 + mh_2 + dT_Q k^2 - \tilde{\beta}\omega)C - mC_{l0},\\
T_{s0} &= (mh_2 + dT_Q k^2 - \tilde{\beta}\omega)C + mC_{l0},\\
\epsilon k T_{s0} &= -\frac{\alpha_h \rho_l c_l u_*}{k_s} T_{l0} - \left(\frac{T_Q \omega}{D_T} + \frac{\alpha_h \rho_l c_l u_* h_1}{k_s}\right) C,\\
C_{l0}\left(1 + \frac{(1-k_0)V\cos\theta}{\alpha_m u_*}\right) &= -\left(\frac{V\cos\theta h_2(1-k_0)}{\alpha_m u_*} + \frac{C_i\omega(1-k_0)}{\alpha_m u_*} + h_2\right) C.
\end{aligned}
\tag{23}
$$

Now substituting T_{l0} and T_{s0} from the first and second lines of equations (23) into the third line, we arrive at

$$
C_{l0}\left(\epsilon k m - \frac{\alpha_h \rho_l c_l u_* m}{k_s}\right) = \left(-\epsilon k m h_2 - \epsilon d T_Q k^3 + \epsilon k \tilde{\beta}\omega + \frac{\alpha_h \rho_l c_l u_*}{k_s}\left(mh_2 + dT_Q k^2 - \tilde{\beta}\omega\right) - \frac{T_Q \omega}{D_T}\right) C. \tag{24}
$$

Combining the fourth line of (23) and (24) (eliminating the perturbation amplitudes C_{l0} and C), we come to a dispersion law for the function $\omega(k)$, which reads as

$$
\begin{aligned}
&-\left(\frac{V\cos\theta h_2(1-k_0)}{\alpha_m u_*} + \frac{C_i\omega(1-k_0)}{\alpha_m u_*} + h_2\right)\left(\epsilon k m - \frac{\alpha_h \rho_l c_l u_* m}{k_s}\right)\\
&= \left(1 + \frac{(1-k_0)V\cos\theta}{\alpha_m u_*}\right)\left(-\epsilon k m h_2 - \epsilon d T_Q k^3 + \epsilon k \tilde{\beta}\omega + \frac{\alpha_h \rho_l c_l u_*}{k_s}\left(mh_2 + dT_Q k^2 - \tilde{\beta}\omega\right) - \frac{T_Q\omega}{D_T}\right).
\end{aligned}
\tag{25}
$$

Next, consider a system of coordinates moving in the direction normal to the dendrite surface with velocity $V\cos\theta$. Due to the rotational symmetry of the system, the perturbation with wavenumber k grows with velocity $\omega(k)$. When the origin of the coordinate system moves along the axis z with a constant velocity V, the perturbation increases as $\omega(k) - iVk\sin\theta$ due to the tangential velocity $V\sin\theta$ in the new coordinate system.[20,36] Consequently, replacing $\omega(k)$ by $-iVk\sin\theta$ on the neutral stability curve (where ω disappears), setting $\epsilon = -1$ and replacing $-i$ instead of i according to the previous theories,[20,36] we arrive at the following equation for the marginal wavenumber $k = k_m$

$$
{k_m}^2 + \left(2b - \frac{i\beta V\sin\theta}{d} - \frac{iB\sin\theta}{dA}\right) k_m - \frac{2bi\beta V\sin\theta}{d} - \frac{iV\sin\theta}{D_T d} - \frac{2biB\sin\theta}{dA} = 0, \tag{26}
$$

where

$$
b = \frac{\alpha_h \rho_l c_l u_* m}{k_s},\ \beta(\theta) = \frac{\tilde{\beta}(\theta)}{T_Q},\ A = 1 + \frac{V\cos\theta(1-k_0)}{\alpha_m u_*},\ B = \frac{mVC_i(1-k_0)}{\alpha_m u_* T_Q}.
$$

4 | SOLVABILITY THEORY

To derive the selection criterion, the limit wavenumber k_m found from Equation (26) is substituted into the following solvability condition derived by Pelcé and Bensimon[19]

$$
\int_{-\infty}^{\infty} G\left[X_0(l)\right] Y_m(l) dl = 0,\ Y_m(l) = \exp\left[i\int_0^l k_m(l_1) dl_1\right], \tag{27}
$$

where G denotes an arbitrary curvature operator, and $X_0(l)$ represents the solution continuum from which the dependence $k_m(l)$ is obtained (here $X_0(l)$ stands for the Ivantsov parabola function of the curvilinear coordinate l). Note that orthogonality of $G\left[X_0(l)\right]$ and $Y_m(l)$ means that steady solutions can be found close to an Ivantsov parabola in the case of small surface tension.

For dendritic growth in a single-component system ($C_{l\infty} = C_i = 0$), the solution of Equation (26) is

$$k = -b + \frac{i\beta V \sin\theta}{2d} - b\sqrt{1 + \frac{iqV\sin\theta}{bd}}, \tag{28}$$

where we suppose that $q = \beta_0 + 1/(bD_T)$, $\alpha_\beta \ll 1$, and $V \lesssim 10$ m/s (or $P_g \lesssim 1$ for typical metallic melts).

By combining expressions (27) and (28) in the case of small anisotropies $\alpha_d \ll 1,\ \alpha_\beta \ll 1$ and assuming $\theta_d = 0$,[19,20] we obtain the following solvability integral

$$\int_{-\infty}^{\infty} d\phi G\left[X_0(\eta(\phi))\right] \exp\left\{\int_{1/\sqrt{2\alpha_d}}^{\phi}\left[\sqrt{\frac{2^{7/4}\rho^2 bqV\alpha_d^{5/n}A_n^{5/n}\left(\phi'^{\frac{n+1}{2}} - \tilde{\tau}\phi'(\phi'^{n/2}-1)\right)}{d_0\left(1-\phi'^{n/2}\right)}}\right.\right.$$
$$\left.\left. + \frac{\rho {A_n}^{2/n}}{\sqrt{2}d_0\alpha_d^{1-2/n}}\left(2^{7/4}\alpha_d^{1+1/n}A_n^{1/n}bd_0\sqrt{\phi'} + \beta_0 V\alpha_\beta\right)\right]d\phi'\right\} = 0, \tag{29}$$

where

$$A_n = 2^{-3n/4}\sum_{k=0}^{n}\binom{n}{k} i^{n-k}\cos\frac{(n-k)\pi}{2},\ \tau = \frac{2^{3/4}\alpha_d^{\frac{5-n}{4}}bd_0}{qV},\ \tilde{\tau} = \tau A_n^{1/n}\alpha_d^{\frac{(n-1)(n-4)}{4n}}.$$

The following substitutions are included in this expression[19,20,36]

$$l_1 = -\frac{\rho}{2}\left[\frac{\tan\theta}{\cos\theta} + \ln\left(\frac{1}{\cos\theta} + \tan\theta\right)\right],\ \eta(\phi) = \tan\theta = i\left(1 - \sqrt{2\alpha_d}\phi\right),\ \phi = \frac{A_n^{2/n}\phi'}{\alpha_d^{(n-4)/(2n)}},\ \alpha_d \approx \alpha_\beta \ll 1.$$

The solvability integral (29) is found in accordance with the previous theoretical works.[9,20,22,36] The method of approximate evaluation of this integral is connected with the determination of main contributions from the first summand in square brackets of (29). These dominant contributions appear from the loop and stationary phase points in the complex plane of integration. The first contribution is calculated between the distance $\sim \tilde{\tau}^{2/3}$ (stationary phase point splitting distance) at the intersection of the steep descent trajectory and the real axis and $\phi' \sim 1$.[22] This contribution can be written as

$$\cos\left[\bar{A}_1\sqrt{\frac{\rho^2 bqV\alpha_d^{5/n}A_n^{5/n}}{d_0}}\left(1 + \bar{B}_1\tilde{\tau}^{\frac{n+5}{2(n-1)}}\right) + \frac{2a_1}{3}\tilde{\tau}^{\frac{3}{n-1}} + a_2\tilde{\tau}^{\frac{2}{n-1}}\right]. \tag{30}$$

The second contribution behaves as an exponential function whose oscillating part has the form

$$\cos\left[\bar{A}_2\sqrt{\frac{\rho^2 bqV\alpha_d^{5/n}A_n^{5/n}}{d_0}}\left(1 + \bar{B}_2\tilde{\tau}^{\frac{n+5}{2(n-1)}}\right) + \frac{2a_{1(1-\tilde{\tau}^{\frac{3}{n-1}})}}{3} + a_2\left(1 - \tilde{\tau}^{\frac{2}{n-1}}\right)\right], \tag{31}$$

$$a_1 = 2^{5/4}A_n^{3/n}\alpha_d^{3/n}\rho b,\ a_2 = \frac{\alpha_\beta A_n^{2/n}\rho\beta_0 V}{\sqrt{2}d_0\alpha_d^{\frac{n-2}{n}}},$$

where $\bar{A}_1$, $\bar{A}_2$, $\bar{B}_1$, and $\bar{B}_2$ are all constans. A more detailed description of the evaluation method can be found in previous works (see, e.g., Bouissou and Pelcé[22]).

Cancelation of the sum of contributions (30) and (31) leads to the convective stability criterion of dendritic growth in an undercooled liquid phase

$$\sigma^* = \frac{2d_0D_T}{\rho^2V} = \frac{\sigma_{0n}\alpha_d^{5/n}A_n^{5/n}(1+bD_T\beta_0)\left(1+\mu_n\tilde{\tau}_n^{\frac{n+5}{2(n-1)}}\right)^2}{\left[1+\nu_{1n}\left(\alpha_d^{3/n}A_n^{3/n}\rho b+\frac{3\alpha_d^{1/4}A_n^{2/n}\rho\beta_0V}{2^{5/4}d_0}\right)\right]^2}. \tag{32}$$

where $\nu_{1n}^2 = 2^{9/2}25\sigma_{0n}/27$, σ_{0n} and μ_n are constants provided from phase field simulations or experimental results.[37–42]

Thermo-solutal growth is considered in the limit of dilute systems, where $\beta_1 \ll \sqrt{d_0/(VD_T)}$ or $\beta_1 \ll bd_0/V$ and $A \sim 1$, the wave number k_m is taken from expression (28), and the parameter β_0 is replaced by $\beta_1 = \beta_0 + mC_i(1-k_0)/(T_Q\alpha_m u_*)$. Note that small β_1 means small kinetic effects compared to capillary. In this case, the selection criterion reads as

$$\sigma^* = \frac{\sigma_{0n}\alpha_d^{5/n}A_n^{5/n}(1+bD_T\beta_1)\left(1+\mu_n\tilde{\tau}_{1n}^{\frac{n+5}{2(n-1)}}\right)^2}{\left[1+\nu_{1n}\left(\alpha_d^{3/n}A_n^{3/n}\rho b+\frac{3\rho\alpha_d^{1/4}A_n^{2/n}\beta_1V}{2^{5/4}d_0}\right)\right]^2},\ \tilde{\tau}_{1n} = \frac{\alpha_d^{1/n}A_n^{1/n}\rho b^2d_0}{2^{1/4}P_g(1+bD_T\beta_1)}. \tag{33}$$

Considering the opposite case $\beta_1 \gg \sqrt{d_0/(VD_T)}$, we obtain the wavenumber from (26) in the form of

$$k = \frac{i\beta_1V\sin\theta}{d}. \tag{34}$$

Combining expressions (27) and (34), we arrive at the solvability integral

$$\int_{-\infty}^{\infty} d\phi G\left[X_0(\eta(\phi))\right]\exp\left(\frac{\sqrt{2}\rho V\beta_1\alpha_d^{2/n}A_n^{2/n}}{d_0}\int_{1/\sqrt{2\alpha_d}}^{\phi}\frac{\phi'^{n/2}d\phi'}{\phi'^{n/2}-1}\right) = 0, \tag{35}$$

where the contribution from the loop can be written as

$$\cos\left(\frac{\bar{A}_3\rho V\beta_1\alpha_d^{2/n}A_n^{2/n}}{d_0}\right) = 0, \tag{36}$$

and $\bar{A}_3$ represents a constant.

Equating (36) to zero, we come to the selection criterion

$$\sigma^* = \frac{2d_0D_T}{\rho^2V} = \frac{2\sigma_{0n}D_T\beta_1\alpha_d^{2/n}A_n^{2/n}}{\rho}, \tag{37}$$

where σ_{0n} is a constant which can be taken from phase field modeling or experimental data (here the limit of suitability is $\beta_1 \gg \sqrt{d_0/(VD_T)}$).

It is significant that σ^* from (33) (derived for $\beta_1 \ll \sqrt{d_0/(VD_T)}$) vanishes in the case of large β_1 whereas σ^* from (37) (derived for $\beta_1 \gg \sqrt{d_0/(VD_T)}$) vanishes in the opposite limiting case. Such a behavior enables us to sew together these asymptotic solutions.

Consequently, the generalized selection criterion for both limiting cases in β_1 can be written as

$$\sigma^*(\rho,V) = \frac{2d_0D_T}{\rho^2V} = \frac{\sigma_{0n}\alpha_d^{5/n}A_n^{5/n}(1+bD_T\beta_1)\left(1+\mu_n\tilde{\tau}_{1n}^{\frac{n+5}{2(n-1)}}\right)^2}{\left[1+\nu_{1n}\left(\alpha_d^{3/n}A_n^{3/n}\rho b+\frac{3\alpha_d^{1/4}A_n^{2/n}P_g\beta_1D_T}{2^{1/4}d_0}\right)\right]^2}+\frac{2\sigma_{0n}\alpha_d^{2/n}A_n^{2/n}D_T\beta_1}{\rho}. \tag{38}$$

TABLE 1 Material and calculation parameters for the alloy Al-24 at. % Ge. Parameters marked by (*) are given by Becker et al[38]

Parameter	Symbol	Value	Units
Solute partition coefficient*	k_0	0.11	—
Liquidus slope*	m	10.4	K/at.%
Hypercooling*	T_Q	353	K
Liquidus temperature*	T_0	732	K
Solute diffusion coefficient*	D_C	$7 \cdot 10^{-9}$	$m^2\ s^{-1}$
Initial composition*	$C_{l\infty}$	24	at.%
Capillary constant*	d_0	$4.3 \cdot 10^{-10}$	m
Thermal diffusivity	D_T	$4 \cdot 10^{-5}$	$m^2\ s^{-1}$
Liquid density	ρ_l	$1.26 \cdot 10^3$	$kg\ m^{-3}$
Heat capacity	c_l	550	$J\ kg^{-1}\ K^{-1}$
Thermal conductivity in the solid	k_s	29.22	$W\ m^{-1}\ K^{-1}$
Friction velocity of flow	u_*	$3.3 \cdot 10^{-4}$	$m\ s^{-1}$
Surface energy stiffness	α_d	0.026	—
Solvability constant	σ_0	0.09	—
Convective coefficient of mass	α_m	2.88	—
Order of crystalline symmetry	n	4	—

The selection criterion (38) is a combination of the dendrite growth velocity V and tip diameter ρ in the case of n-fold symmetry and convective heat and mass transfer in the liquid phase.

The undercooling balance ΔT provides a second combination of growth velocity and the tip diameter. This combination yields solutions close to the stationary Ivantsov or Horvay–Chan solutions, which determine the temperature and concentration around the dendrite surface. Considering the case of convective boundary conditions (4) and (5) at the dendrite surface, we come to

$$\Delta T = \Delta T_T + \Delta T_C + \Delta T_R + \Delta T_K. \tag{39}$$

Here, the thermal ΔT_T, concentration ΔT_C, curvature ΔT_R, and kinetics ΔT_K contributions read as

$$\Delta T_T = T_i - T_\infty = \frac{T_Q V k_s}{\alpha_h \rho_l c_l u_* D_T},\ \Delta T_C = m(C_i - C_{l\infty}) = \frac{(1-k_0)VmC_{l\infty}}{\alpha_m u_* - (1-k_0)V},$$
$$\Delta T_R = \frac{4 d_0 T_Q}{\rho},\ \Delta T_K = \frac{V}{\mu_k}, \tag{40}$$

where the previously mentioned analytical solutions (10)–(15) are taken into account.

5 | A TEST OF THEORY AGAINST EXPERIMENTAL DATA FOR AN AL-GE ALLOY

The system of two transcendental equations (selection criterion (38) and undercooling balance (39)) defines the dendrite tip velocity V and tip diameter ρ as functions of total undercooling ΔT. In this section, we compare this solution and previous theoretical predictions under conductive boundary conditions[36] with experimental data[38] obtained for the alloy Al-24 at. % Ge (material and calculation parameters are given in Table 1). To do this, we solved the nonlinear systems of selection criterion and undercooling balance for convective (the case under consideration) and conductive (previously developed theory[36]) boundary conditions using MATLAB computing platform.

The solidification experiments with Al-24 at. % Ge alloys[38] were carried out using a horizontal sample alignment, minimizing gravity-induced fluid flow. The driving force for solidification is the total undercooling ΔT at the dendrite tip. It is defined as the sum of solutal and curvature (Gibbs–Thomson effect) undercooling; kinetic and thermal undercooling were neglected, as fast thermal diffusion was assumed (i.e., $\Delta T_T = 0$ and $\Delta T_K = 0$).

Figure 3 compares the model predictions for convective and conductive boundary conditions with experimental data on dendrite growth velocity. It can be seen that conductive theory[36] well describes experimental data in the intermediate undercooling region, $3\ \mathrm{K} < \Delta T < 8\ \mathrm{K}$, which is in good agreement with the isothermal version of the Lipton–Glicksman–Kurz (LGK) model used for the calculations by Becker et al.[38] In the low undercooling region, $\Delta T < 3\ \mathrm{K}$, distinct deviations from predictions of both conductive and LGK model[38] occur. During dendrite growth, convection

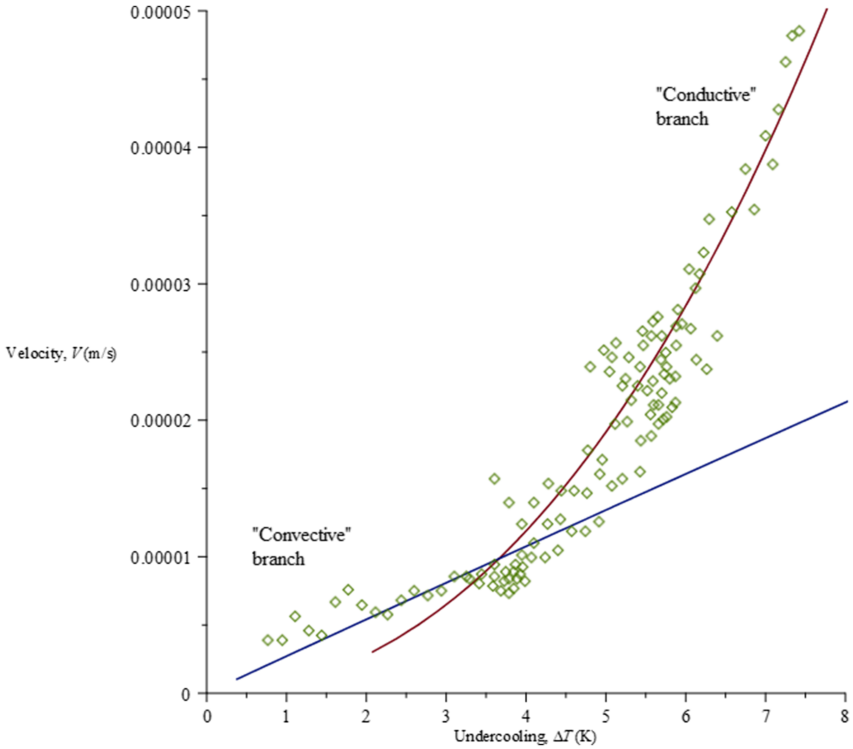

FIGURE 3 Dendrite tip velocity V as a function of melt undercooling ΔT for the alloy Al-24 at. % Ge. (experimental points from Becker et al[38])

at the crystaal tip can play a pronounced role. Despite the fact that the gravity-driven fluid flow was minimized in experiments, convection in front of the tips is still possible. In this case, we have assumed that the fluid flow in the levitated droplets is intense (turbulent), so that intense swirls leading to convective mass transfer occur at the growing dendrite tips. Thus, it can be clearly seen that including the convective boundary conditions (expressions 4 and 5) extends the range of reliable model predictions to low undercoolings. It is also important that the crystallization velocity V grows faster with undercoling in the case of conductive mechanism of heat and mass transfer (Figure 3). In other words, convective transport of heat and mass near dendrites caused, for example, by turbulence dilutes the melt undercooling and inhibits dendrite growth.

6 | CONCLUSION

A theoretical model based on the solvability theory and morphological stability analysis selecting a stable dendritic growth mode in the case of intense fluid flow is developed. A new nonlinear equation for the marginal wavenumber limit is derived and solved for various solidification scenarios. In combination with the solvability theory, we derived a new stability (solvability) criterion representing a relation between dendrite growth velocity, tip diameter, and melt undercooling. Keeping the undercooling balance in consideration, the second relation between these parameters, we derived a closed set of nonlinear algebraic equations that describe the governing dependencies $V(\Delta T)$ and $\rho(\Delta T)$. These functions characterize the material microstructure and structural transformations in the solidified substance. Our analysis stitched together with a model for conductive boundary conditions demonstrates excellent agreement between the theory and experimental data in the entire range of melt undercooling. At a low undercooling, the growth is well described by the convective-type selection criterion under study, whereas at the moderate or high undercooling, conductive heat and mass transfer prevails.

It is well-known that there exist solidification processes where directional and equiaxed solidification can occur simultaneously, e.g., when nucleation, growth, and coalescence of solid microstructural features occur at the same time. In such situations, the released latent heat of fusion can interact with dendrite growth and change all operational and microstructural characteristics of solidified materials. Examples are porosity, interdendritic spacing, microstructural transitions between polycrystalline and single-crystalline structures, and so on. A study of such synchronous occurrence of directional and equiaxed phase transitions is a challenging task for future studies that can be investigated with allowance for the theories of dendrite growth and mushy zone dynamics.[43–55]

ACKNOWLEDGEMENT

L.V.T. acknowledges financial support from the Ministry of Science and Higher Education of the Russian Federation (project 075-02-2021-1387 for the development of the regional scientific and educational mathematical center "Ural Mathematical Center") for the linear stability analysis. Moreover, she is grateful to the Foundation for the Advancement of Theoretical Physics and Mathematics "BASIS" (project No. 21-1-3-11-1) for the development of solvability theory. P.K.G. and D.V.A. acknowledge the Russian Science Foundation (Project No. 21-19-00279) for the stitching of selection criteria, computer simulations, and comparison with experimental data. Open Access funding enabled and organized by Projekt DEAL.

AUTHOR CONTRIBUTION

The authors contributed equally to the present research article.

CONFLICT OF INTEREST

The authors declare no potential conflict of interests.

ORCID

Liubov V. Toropova https://orcid.org/0000-0003-4587-2630
Markus Rettenmayr https://orcid.org/0000-0003-4721-5087
Peter K. Galenko https://orcid.org/0000-0003-2941-7742
Dmitri V. Alexandrov https://orcid.org/0000-0002-6628-745X

REFERENCES

1. Trivedi R, Kurz W. Dendritic growth. *Int Mater Rev*. 1994;39:49-74.
2. Kurz W, Fisher DJ. *Fundamentals of Solidification*. Aedermannsdorf: Trans. Tech. Publ. 1989.
3. Herlach D, Galenko P, Holland-Moritz D. *Metastable Solids from Undercooled Melts*. Amsterdam: Elsevier; 2007.
4. Galenko PK, Alexandrov DV. From atomistic interfaces to dendritic patterns. *Phil Trans R Soc A*. 2018;376:20170210.
5. Alexandrov DV, Zubarev AYu. Heterogeneous materials: metastable and non-ergodic internal structures. *Phil Trans R Soc A*. 2019;377:20180353.
6. Alexandrov DV, Zubarev AYu. Patterns in soft and biological matters. *Phil Trans R Soc A*. 2020;378:20200002.
7. Alexandrov DV, Zubarev AYu. Transport phenomena in complex systems (part 1). *Phil Trans R Soc A*. 2021;379:20200301.
8. Gusakova OV, Galenko PK, Shepelevich VG, Alexandrov DV, Rettenmayr M. Diffusionless (chemically partitionless) crystallization and subsequent decomposition of supersaturated solid solutions in Sn-Bi eutectic alloy. *Phil Trans R Soc A*. 2019;377:20180204.
9. Alexandrov DV, Galenko PK. Dendrite growth under forced convection: analysis methods and experimental tests. *Phys-Usp*. 2014;57:771-786.
10. Worster MG. Natural convection in a mushy layer. *J Fluid Mech*. 1991;224:335-359.
11. Somboonsuk K, Mason JT, Trivedi R. Interdendritic spacing: part i. experimental studies. *Metall Trans A*. 1984;15A:967-975.
12. Trivedi R. Interdendritic spacing: part ii. a comparison of theory and experiment. *Metall Trans A*. 1984;15A:977-982.
13. Alexandrov DV, Britousova AV. Interdendritic spacing in growth processes with a mushy layer. *AIP Conf Proc*. 2015;1648:850101.
14. Alexandrov DV, Bashkirtseva IA, Ryashko LB. Nonlinear dynamics of mushy layers induced by external stochastic fluctuations. *Phil Trans R Soc A*. 2018;376:20170216.
15. Nizovtseva IG, Alexandrov DV. The effect of density changes on crystallization with a mushy layer. *Phil Trans R Soc A*. 2020;378:20190248.
16. Alexandrova IV, Alexandrov DV, Aseev DL, Bulitcheva SV. Mushy layer formation during solidification of binary alloys from a cooled wall: The role of boundary conditions. *Acta Physica Polonica A*. 2009;115(4):791-794.
17. Alexandrov DV, Malygin AP. Flow-induced morphological instability and solidification with the slurry and mushy layers in the presence of convection. *Int J Heat Mass Trans*. 2012;55:3196-3204.
18. Langer JS, Hong DC. Solvability conditions for dendritic growth in the boundary-layer model with capillary anisotropy. *Phys Rev A*. 1986;34:1462-1471.
19. Pelcé P, Bensimon D. Theory of dendrite dynamics. *Nucl Phys B*. 1987;2:259-270.
20. Pelcé P. *Dynamics of Curved Fronts*. Boston: Academic Press; 1987.
21. Ben Amar M, Pelcé P. Impurity effect on dendritic growth. *Phys Rev A*. 1989;39:4263-4269.
22. Bouissou P, Pelcé P. Effect of a forced flow on dendritic growth. *Phys Rev A*. 1989;40:6673-6680.
23. Alexandrov DV, Galenko PK. Selection criterion of stable dendritic growth at arbitrary péclet numbers with convection. *Phys Rev E*. 2013;87:62403.

24. Alexandrov DV, Galenko PK. Thermo-solutal and kinetic regimes of an anisotropic dendrite growing under forced convective flow. *Phys Chem Chem Phys*. 2015;17:19149-19161.
25. Alexandrov DV, Galenko PK. Selection criterion of stable mode of dendritic growth with n-fold symmetry at arbitrary péclet numbers with a forced convection. In: Gutschmidt S, Hewett JN, Sellier M, eds. *Iutam Symposium on Recent Advances in Moving Boundary Problems in Mechanics*, IUTAM Bookseries 34: Springer; 2019:203-215.
26. Alexandrov DV, Galenko PK. Selected mode for rapidly growing needle-like dendrite controlled by heat and mass transport. *Acta Mater*. 2017;137:64-70.
27. Galenko PK, Alexandrov DV, Titova EA. The boundary integral theory for slow and rapid curved solid/liquid interfaces propagating into binary systems. *Phil Trans R Soc A*. 2018;376:20170218.
28. Alexandrov DV, Galenko PK. Selected mode of dendritic growth with n-fold symmetry in the presence of a forced flow. *EPL*. 2017;119:16001.
29. Alexandrov DV, Galenko PK. A review on the theory of stable dendritic growth. *Phil Trans R Soc A*. 2021;379:20200325.
30. Notz D, McPhee MG, Worster MG, Maykut GA, Schlünzen KH, Eicken H. Impact of underwater-ice evolution on arctic summer sea ice. *J Geophys Res*. 2003;108:3223.
31. McPhee MG, Maykut GA, Morison GH. Dynamics and thermodynamics of the ice/upper ocean system in the marginal ice zone of the greenland sea. *J Geophys Res*. 1987;92:7017-7031.
32. Alexandrov DV, Nizovtseva IG. Nonlinear dynamics of the false bottom during seawater freezing. *Dokl Earth Sci*. 2008;419:359-362.
33. Alexandrov DV, Nizovtseva IG. To the theory of underwater ice evolution, or nonlinear dynamics of 'false bottoms'. *Int J Heat Mass Trans*. 2008;51:5204-5208.
34. Herlach DM, Galenko PK. Rapid solidification: in situ diagnostics and theoretical modelling'. *Mater Sci Eng A*. 2007;449-451:34-41.
35. LeadEx Group T. The LeadEx experiment. *EOS Trans AGU*. 1993;74(35):393-400.
36. Alexandrov DV, Galenko PK, Toropova LV. Thermo-solutal and kinetic modes of stable dendritic growth with different symmetries of crystalline anisotropy in the presence of convection. *Phil Trans R Soc A*. 2018;376:20170215.
37. Tong X, Beckermann C, Karma A, Li Q. Phase-field simulations of dendritic crystal growth in a forced flow. *Phys Rev E*. 2001;63:061601.
38. Becker M, Klein S, Kargl F. Free dendritic tip growth velocities measured in al-ge. *Phys Rev Mat*. 2018;2:073405.
39. Jeong J-H, Goldenfeld N, Dantzig JA. Phase fieldmodel for three-dimensional dendritic growth with fluid flow. *Phys Rev E*. 2001;64:041602.
40. Teraoka Y, Saito A, Okawa S. Ice crystal growth in supercooled solution. *Int J Refrig*. 2002;25:218-225.
41. Titova EA, Alexandrov DV, Galenko PK. Selection constants in the theory of stable dendritic growth. *Eur Phys J Special Topics*. 2020;229:2891-2897.
42. Kao A, Toropova LV, Krastins I, Demange G, Alexandrov DV, Galenko PK. A stable dendritic growth with forced convection: a test of theory using enthalpy-based modeling methods. *JOM*. 2020;72:3123-3131.
43. Alexandrova IV, Alexandrov DV. Dynamics of particulate assemblages in metastable liquids: A test of theory with nucleation and growth kinetics. *Phil Trans R Soc A*. 2020;378:20190245.
44. Hills RN, Loper DE, Roberts PH. A thermodynamically consistent model of a mushy zone. *Q J Appl Maths*. 1983;36:505-539.
45. Fowler AC. The formation of freckles in binary alloys. *IMA J Appl Math*. 1985;35:159-174.
46. Borisov VT. *Theory of Two-Phase Zone of a Metal Ingot*. Moscow: Metallurgiya Publishing House; 1987.
47. Alexandrov DV, Ivanov AA, Alexandrova IV. Analytical solutions of mushy layer equations describing directional solidification in the presence of nucleation. *Phil Trans R Soc A*. 2018;376:20170217.
48. Ivanov AA, Alexandrova IV, Alexandrov DV. Phase transformations in metastable liquids combined with polymerization. *Phil Trans R Soc A*. 2019;377:20180215.
49. Barbieri A, Langer JS. Predictions of dendritic growth rates in the linearized solvability theory. *Phys Rev A*. 1989;39:5314-5325.
50. Tritton DJ. *Physical Fluid Dynamics*. Oxford, UK: Clarendon Press; 1988.
51. Toropova LV, Alexandrov DV, Galenko PK. Convective and conductive selection criteria of a stable dendritic growth and their stitching. *Math Meth Appl Sci*. 2020;44(16):12139-12151.
52. Kao A, Toropova LV, Alexandrov DV, Demange G, Galenko PK. Modeling of dendrite growth from undercooled nickel melt: Sharp interface model versus enthalpy method. *J Phys Condens Matter*. 2020;32(19):194002.
53. Toropova LV, Alexandrov DV, Rettenmayr M, Galenko PK. The role of intense convective flow on dendrites evolving with n-fold symmetry. *J Cryst Growth*. 2020;535:125540.
54. Toropova LV, Galenko PK, Alexandrov DV, Demange G, Kao A, Rettenmayr M. Theoretical modeling of crystalline symmetry order with dendritic morphology. *Eur Phys J Special Topics*. 2020;229(2-3):275-286.
55. Toropova LV, Galenko PK, Alexandrov DV, Rettenmayr M, Kao A, Demange G. Non-axisymmetric growth of dendrite with arbitrary symmetry in two and three dimensions: sharp interface model vs phase-field model. *Eur Phys J Special Topics*. 2020;229(19-20):2899-2909.

How to cite this article: Toropova LV, Rettenmayr M, Galenko PK, Alexandrov DV. Mathematical modeling of dendrite growth in an Al–Ge alloy with convective flow. *Math Meth Appl Sci*. 2021;1-13. doi:10.1002/mma.7991